Inorganic Chemistry

Article

pubs.acs.org/IC

High-Resolution Spectroscopy and Structure of Osmium Tetroxide. A Benchmark Study on $^{192}OsO_4$

Maud Louviot,*[,†] Vincent Boudon,[†] Laurent Manceron,[‡,§] Pascale Roy,[§] Dionisio Bermejo,[⊥] and Raúl Z. Martínez[⊥]

[†]Laboratoire Interdisciplinaire Carnot de Bourgogne (ICB), CNRS UMR 6303, Université de Bourgogne, 9 Avenue Alain Savary, BP 47870, F-21078 Dijon Cedex, France

[‡]Laboratoire de Dynamique, Interactions et Réactivité, CNRS UMR 7075, 4 Place Jussieu, F-75252 Paris Cedex, France

[§]Synchrotron SOLEIL, Ligne AILES, L'Orme des Merisiers Saint-Aubin, F-91192 Gif-sur-Yvette, France

[⊥]Instituto de Estructura de la Materia, CSIC, Serrano 123, 28006 Madrid, Spain

ABSTRACT: Osmium tetroxide (OsO_4) is a heavy tetrahedral molecule that constitutes a benchmark for quantum chemistry calculations. Its favorable spin statistics (due to the zero nuclear spin of oxygen atoms) is such that only A_1 and A_2 (T_d symmetry) rovibrational levels are allowed, leading to a dense but quite easily resolvable spectrum. We reinvestigate here the ν_1/ν_3 stretching fundamental (940−980 cm^{-1}) dyad region and perform new assignments and effective Hamiltonian parameter fits for the main isotopologue ($^{192}OsO_4$). We also investigate the ν_2/ν_4 bending fundamental dyad (300−360 cm^{-1}) for the first time and perform a preliminary analysis. New experimental data have been obtained at 0.001 cm^{-1} resolution using an isotopically pure $^{192}OsO_4$ sample and the Synchrotron SOLEIL light source. Assignments and analyses were performed using *SPVIEW* and *XTDS* software, respectively. We provide precise effective Hamiltonian parameters, including the band centers for all of the fundamental levels and rotational constants for the ground state and for all four fundamental levels. We discuss isotopic shifts, estimate the equilibrium rotational constant B_e, and derive a precise value for the equilibrium bond length r_e(Os−O) = 1.70919(16) Å. We also performed experiments to measure for the first time the IR integrated intensities for the ν_2/ν_4 bending fundamental dyad. These new data are compared to current ab initio predictions.

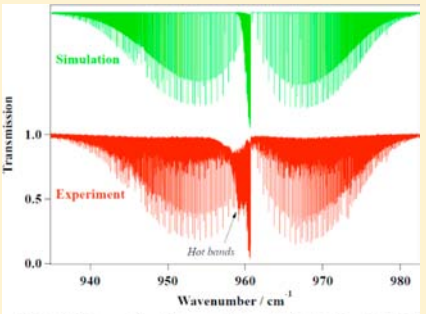

Overview of the ν_1/ν_3 infrared region compared to the simulation.

INTRODUCTION

Osmium tetroxide (OsO_4) is one of the three known oxides in which the heavy element exists in the highest possible oxidation state. Osmium is an element that is found in very small quantities in nature, amid other noble metals. Therefore, one could expect that osmium compounds would rank among exotic molecules, without much practical importance. This is, however, not the case, because of several remarkable physical and chemical properties. First and foremost is the high volatility of OsO_4 (near 10 mbar at room temperature) for a compound having such a heavy mass, together with a relative thermodynamic stability, which makes this rare compound a polluting agent[1−4] (issued as a byproduct from catalytic exhaust pipes in cars[5]) and a potential warfare agent.[6] Its chemical application as a reagent and a catalyst for olefin hydroxylation,[7] as well as its use as a contrast enhancer for electron microscopy,[8] is well-known because it serves as a staining agent for certain lipids[9] or as an oxidizing agent.[10] It can also modify the electrical properties of some nanomaterials,[11,12] and, as such, it helped to understand the structure of the C_{60} fullerene.[13] More relevant here, it is also an important benchmark molecule for modeling relativistic effects in systems containing heavy elements.[14]

Many molecular properties, such as electronic and geometrical structures, electrical properties, thermodynamic and adsorption stabilities, and reactivity, are deeply affected by relativistic effects, and a large body of theoretical studies is devoted to devising and assessing methods to account for these effects. Many recent studies refer to OsO_4 for modeling important measurable molecular properties.[15−21] With no permanent dipole moment, no pure rotational spectroscopy has yet been recorded, and the existing structural experimental data have been obtained by X-ray diffraction,[22] electron diffraction,[23] and, more recently, extended X-ray absorption fine structure (EXAFS).[24] X-ray diffraction data have indicated a 1.74(2) Å bond length with a slight (0.03 Å) asymmetry caused by short-range molecular interactions, but electron diffraction and EXAFS data on diluted molecules converged toward a 1.712(3) Å value. These values rely in all cases upon various approximations to account for thermal excitation effects (only about 30% of the molecules are in their ground state at room temperature; see below) and, thus, it seems desirable to obtain more accurate structural data for the ground state, or even better, corrected for zero-point energy effects to

Received: July 13, 2012
Published: September 20, 2012

   dx.doi.org/10.1021/ic3015282 | *Inorg. Chem.* 2012, 51, 10356−10365

enable a rigorous comparison with quantum-chemical calculations.

OsO_4, just like CH_4 and other tetrahedral spherical top molecules pertaining to the T_d point group, has four normal modes of vibration: one nondegenerate mode with A_1 symmetry (ν_1), one doubly degenerate mode with E symmetry (ν_2), and two triply degenerate modes with F_2 symmetry (ν_3 and ν_4). Only F_2 fundamental states are IR-active, in a first approximation, but the other modes can gain some absorption intensity through rovibrational couplings. The ν_1 and ν_3 stretching fundamental wavenumbers are close to each other (966.69 and 960.74 cm^{-1}, respectively), while the ν_2 and ν_4 bending fundamental wavenumbers are even closer to each other and are roughly 3 times lower (332.14 and 327.84 cm^{-1}, respectively). This leads to a vibrational polyad structure that we will discuss later in the Theoretical Model section.

IR and Raman spectroscopies had been early applied to the study of this molecule first to confirm its tetrahedral shape, then to assess its force field, and finally to use in metrological applications. In the 1970s, McDowell and Goldblatt[25] and, later, Bobin et al.[26] obtained high-resolution (HR) data on the strongly IR-absorbing ν_3 stretching fundamental. However, because of the specific selection rules for spherical top molecules, a direct determination of the rotational constants of the ground state and vibrational excited states was not possible from analysis of only a degenerate fundamental as an isolated band. Recently, with the advent of third-generation synchrotron radiation (SR) sources of high brightness and stability, recording of HR absorption data for the weaker bending fundamentals in the far-IR has become possible.[27] This, combined with HR Raman measurements of the totally symmetric stretching mode,[28] opened the door for a comprehensive spectroscopic study of OsO_4, for characterization of the molecular parameters in all four first vibrational levels and in the ground state, and thus for an accurate determination of the molecular structure. As a secondary goal, we determined the integrated IR intensities (not yet known for the bending region) and compared them to the existing ab initio predictions.

EXPERIMENTAL DETAILS

$^{192}OsO_4$ Synthesis. Pure, isotopically enriched $^{192}OsO_4$ was synthesized by oxidation of an ^{192}Os-enriched osmium powder (Eurisotop, 99% ^{192}Os, 500 μm particle size) in pure oxygen gas (Air Liquide, Saclay, France, 99.999%, 700 mbar) at about 400 °C in a special glass reactor combined with a liquid-nitrogen trap. The reaction vessel was thoroughly outgassed under high vacuum before use, and the product was distilled under vacuum with trap-to-trap distillation. The absence of air or other lighter byproducts and the sample purity were checked by mass and IR spectroscopy. The sample vapor pressure (13 mbar near 25 °C) was checked with respect to well-known literature data.[29]

HR IR Spectra. Most spectroscopic data have been collected at the French Synchrotron facility SOLEIL on the Infrared Beamline AILES[30,31] using a Bruker IFS 125 HR Fourier transform infrared spectrometer. The brightness of the SR was crucial for obtaining a high signal-to-noise ratio at HR in the far-IR region. Several spectra have been acquired at HR (Bruker "resolution" = $0.9/\Delta_{max}$ = 0.00102 cm^{-1}, where Δ_{max} = 882 cm) for an isotopically pure $^{192}OsO_4$ vapor sample. The goal was 2-fold: first, to obtain the best possible HR spectrum for the ν_2/ν_4 region of $^{192}OsO_4$ and, second, to compare measurements made using SR with or without an aperture stop of the nominal diameter at the spectrometer entrance. We thus checked that, using the SR source, measurements performed with and without the nominal diameter iris (1.5 mm diameter) did not affect the measured line shape and intensities, as was already observed in other spectral domains.[32]

Far-IR measurements were obtained with a 20 cm base length multipass cell and a 805 cm optical path length ($^{192}OsO_4$ data). Measurements were made with a composite Mylar/Si beamsplitter and IR lab high-speed composite bolometer (1 kHz cut off) with a 680 cm^{-1} low-pass optical filter, at 5.06 cm s^{-1} interferometer optical velocity and boxcar apodization. A second, 30-cm-long single-pass gas cell was placed in parallel with the first cell for mid-IR HR measurements on the strongly absorbing ν_1/ν_3 stretching fundamental dyad. Measurements in the 900 cm^{-1} region were made using the Globar internal light source of the spectrometer, a HgCdTe narrow band detector with a 1200−700 cm^{-1} optical filter, a KBr/Ge beamsplitter, and 2.53 cm s^{-1} interferometer optical velocity.

Gas pressures were measured with thermostated capacitive gauges (Pfeiffer, 10 and 1000 mbar heads).

The spectra were calibrated with residual H_2O and CO_2 lines observed in the spectra between 300 and 700 cm^{-1}, with their wavenumbers taken from *HITRAN04*.[33] The spectral calibration is accurate to about 0.0001 cm^{-1} (root mean square, rms).

Low-Resolution IR Spectra. To obtain reliable integrated intensities of the ν_2/ν_4 bands, additional spectra of natural OsO_4 were measured at 0.0102 cm^{-1} resolution for four different pressures (0.497, 0.798, 1.201, and 1.797 mbar) with a 10 mbar capacitive gauge and the cell optical path length adjusted to 565 cm. Nitrogen gas (99.99%, purified through a cold trap) was introduced at a slow flow rate through a liquid-nitrogen trap with increasing pressure (up to 600 mbar of N_2, measured with a 1000 mbar capacitive gauge) until complete blending of the rotational structure was obtained, to achieve a reliable intensity measurement. Note that a pressure of at least 500 mbar was found to be necessary, even at 0.01 cm^{-1} resolution (see Figure 1).

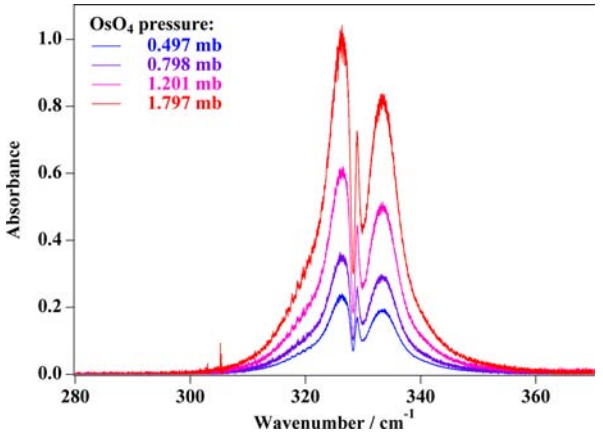

Figure 1. IR spectra (0.01 cm^{-1} resolution) for various OsO_4 pressures (0.497, 0.798, 1.201, and 1.797 mbar) in the 300−350 cm^{-1} ν_2/ν_4 region with 600 mbar of N_2 broadening gas and a 565 cm optical path length. The spike near 307 cm^{-1} is due to a small residual modulation in the SR intensity.

Care was taken to avoid water contamination and to remain at absorbance values between 0.1 and 1 to ensure optimal detection linearity. The spectra were recorded at a 296 ± 1 K temperature.

HR Stimulated Raman Spectrum. A Raman spectral analysis of the ν_1 band was necessary in order to complete our global study on OsO_4 fundamentals. Indeed, considering the geometry of the molecule, the totally symmetric ν_1 (A_1) fundamental is not IR-active but is Raman-active. In our first study,[27] we determined ν_1 Hamiltonian parameters thanks to the second-order Coriolis coupling between the ν_1 and ν_3 bands. The resulting values were reasonable but not fully reliable. The Raman study was thus required to obtain more precise values by performing a simultaneous fit of both IR and Raman lines (see the Analysis section).

The ν_1 Raman spectrum was recorded at Instituto de Estructura de la Materia, Madrid, Spain, from a natural abundance sample. The experimental setup can be found in the recent work by Di Lonardo et

dx.doi.org/10.1021/ic3015282 | Inorg. Chem. 2012, 51, 10356−10365

al.,[34] and the principle of measurement was detailed in our last article.[28] Shortly, a Raman signal is emitted when the frequency difference between a pump laser—here, a pulsed dye laser—and a probe laser—here, a cw Ar^+—corresponds to an active Raman resonance of the molecule. The sample cell was a standard 92-cm-long stainless steel cylinder, and the measurements were conducted at room temperature and at a sample pressure of 7 mbar.

THEORETICAL MODEL

The theoretical model described below to develop the Hamiltonian operator is based on the tensorial formalism and vibrational extrapolation methods used in Dijon, France. It is rather sophisticated because the detailed spectroscopic study of such a highly symmetrical molecule requires the use of advanced mathematical tools of group theory. These methods have already been explained for example in refs 29, 35, and 36. We only recall here the basic principles and their application to the case of OsO_4.

If we consider an XY_4 molecule for which the vibrational levels are grouped into a series of polyads designed by P_k ($k = 0, ..., n$), with P_0 being the ground state (GS), the Hamiltonian operator can be put in the following form (after performing some contact transformations):

$$\mathcal{H} = \mathcal{H}_{\{P_0 \equiv \mathrm{GS}\}} + \mathcal{H}_{\{P_1\}} + ... + \mathcal{H}_{\{P_k\}} + ... + \mathcal{H}_{\{P_{n-1}\}} + \mathcal{H}_{\{P_n\}} \quad (1)$$

Terms like $\mathcal{H}_{\{P_k\}}$ contain rovibrational operators that are specific to polyad P_k. They have no matrix element within the $P_{k'>k}$ basis sets. The effective Hamiltonian for polyad P_n is obtained by projecting $\mathcal{H}$ into the P_n Hilbert subspace, i.e.

$$\begin{aligned} H^{\langle P_n \rangle} &= P^{\langle P_n \rangle} \mathcal{H} P^{\langle P_n \rangle} \\ &= H^{\langle P_n \rangle}_{\{\mathrm{GS}\}} + H^{\langle P_n \rangle}_{\{P_1\}} + ... + H^{\langle P_n \rangle}_{\{P_k\}} + ... + H^{\langle P_n \rangle}_{\{P_{n-1}\}} + H^{\langle P_n \rangle}_{\{P_n\}} \end{aligned} \quad (2)$$

The different terms are expanded in the form

$$\mathcal{H}_{\{P_k\}} = \sum_{\text{all indexes}} t^{\Omega(K,n\Gamma)\Gamma_v\Gamma'_v}_{\{s\}\{s'\}} \beta [V^{\Omega_v(\Gamma_v\Gamma'_v)\Gamma}_{\{s\}\{s'\}} \otimes R^{\Omega(K,n\Gamma)}]^{(A_1)} \quad (3)$$

In this formula, $t^{\Omega(K,n\Gamma)\Gamma_v\Gamma_{v'}}_{\{s\}\{s'\}}$ are the parameters to be determined, while ${}^{\varepsilon}V^{\Omega_v(\Gamma_v\Gamma_{v'})\Gamma}_{\{s\}\{s'\}}$ and $R^{\Omega(K,n\Gamma)}$ are vibrational and rotational operators. They are symmetrized polynomials of elementary vibrational (creation and annihilation) and rotational (angular momentum components) operators. Their respective degrees are Ω_v and Ω. Their construction is described in ref 35. Again, the vibrational operators only have matrix elements within the $P_{k' \le k}$ basis sets. β is a factor that allows the scalar terms ($\Gamma = A_1$) to match the usual terms like $B_0 J^2$ (rigid rotor term), etc. The order of each individual term is defined as $\Omega + \Omega_v - 2$.

Such a Hamiltonian development scheme enables the treatment of any polyad system. With the ν_1 and ν_3 harmonic wavenumbers being close to each other, as mentioned above, the two stretching fundamentals form a ν_1/ν_3 dyad. In a first step, we neglect the influence of the ν_2 and ν_4 bending modes, whose harmonic wavenumbers are roughly 3 times lower. We can thus consider, for the 960 cm^{-1} region spectral analysis, a polyad system (the stretching mode scheme) including the GS and the $\nu_1 = 1$ and $\nu_3 = 1$ vibrational levels together. This allows us to perform a global fit of the effective Hamiltonian parameters for those stretching levels. In the same way, we define another polyad system (the bending mode scheme), including the GS and the $\nu_2 = 1$ and $\nu_4 = 1$ vibrational levels together, because here the ν_2/ν_4 bending dyad is studied separately. Thus, we need the following effective Hamiltonians:

(i) The GS (polyad P_0) effective Hamiltonian

$$H^{\langle \mathrm{GS} \rangle} = H^{\langle \mathrm{GS} \rangle}_{\{\mathrm{GS}\}} \quad (4)$$

(ii) The ν_1/ν_3 stretching dyad (P_1 polyad in the stretching mode scheme) effective Hamiltonian

$$H^{\langle \nu_1/\nu_3 \rangle} = H^{\langle \nu_1/\nu_3 \rangle}_{\{\mathrm{GS}\}} + H^{\langle \nu_1/\nu_3 \rangle}_{\{\nu_1/\nu_3\}} \quad (5)$$

(iii) The ν_2/ν_4 bending dyad (P_1 polyad in the bending mode scheme) effective Hamiltonian

$$H^{\langle \nu_2/\nu_4 \rangle} = H^{\langle \nu_2/\nu_4 \rangle}_{\{\mathrm{GS}\}} + H^{\langle \nu_2/\nu_4 \rangle}_{\{\nu_2/\nu_4\}} \quad (6)$$

A dipole moment operator for ν_1/ν_3 and another one for ν_2/ν_4 are developed in the same way (see, for instance, ref 35 for details about their construction). In the present work, the dipole moment is expanded at the lowest order for both dyads, giving only one parameter in each case, which is the dipole moment derivative of ν_3 and the dipole moment derivative of ν_4, respectively.

We use two vibrational bases, one restricted to the stretching modes and the other one restricted to the bending modes:

$$|(\Psi^{(A_1)}_{\nu_1=1} \otimes \Psi^{(l_3=1,F_2)}_{\nu_3=1})^{(C_v)}\rangle, \qquad |(\Psi^{(l_2=1,E)}_{\nu_2=1} \otimes \Psi^{(l_4=1,F_2)}_{\nu_4=1})^{(C_v)}\rangle \quad (7)$$

That is, we use a three-dimensional harmonic oscillator wave function for the triply degenerate modes ν_3 and ν_4 with vibrational angular momentum l_3 and l_4, a two-dimensional one for the doubly degenerate mode ν_2, and a one-dimensional one for the mode ν_1. The Hamiltonian and dipole moment matrix elements are calculated on the coupled rovibrational basis:

$$|[\Psi^{(C_v)}_v \otimes \Psi^{(J,nC_r)}_r]^{(C)}\rangle \quad (8)$$

with $\Psi^{(J,nC_r)}_r$ being a rotational wave function with angular momentum J, rotational symmetry species C_r, and multiplicity index n (see ref 35), while C is the overall symmetry species ($C = C_v \otimes C_r$). $\Psi^{(C_v)}_v$ is one of the two vibrational basis sets from eq 7.

ANALYSIS

As was stated in the Introduction, the aim of this work is to use HR molecular spectroscopy to perform a rigorous analysis and modeling that leads to a precise determination of the molecular equilibrium structure of $^{192}OsO_4$. This provides an accurate structural parameter that will constitute a benchmark for high-level quantum-chemistry calculations on species containing a heavy atom. We thus detail here the analysis of the stretching and bending dyads using the theory presented in the previous section.

Stretching Dyad Analysis. The aim of this first part of the study is the refinement of the ν_3 parameters determined in our previous work.[27] Because we use here a monoisotopic sample, we obtain a much less congested spectrum; moreover, at high J values, line clusters for the different isotopologues were overlapping each other for the natural abundance spectrum, which is not the case here. It is thus possible to perform more assignments of rotationally high excited states.

A preliminary simulation of the ν_1/ν_3 dyad was performed with *XTDS* software[37] using the $^{192}OsO_4$ ν_3 parameters from our IR multiisotopic study[27] and the ν_1 parameters determined through our Raman study.[28] This allowed us to make a first set of line

dx.doi.org/10.1021/ic3015282 | Inorg. Chem. 2012, 51, 10356−10365

assignments using *SPVIEW* software,[37] i.e., to match experimental lines with theoretical lines. This step was particularly easy because the simulation was similar to that of our multiisotopic study[27] and there was no overlap with the contribution of other isotopologues in the spectrum. Then, we performed a nonlinear least-squares fit of the effective Hamiltonian parameters with *XTDS* software (using a Levenberg–Marquardt algorithm) in order to determine new precise values and to obtain a new simulation so that the difference in the positions of the theoretical and experimental lines was as small as possible. This fit took into account the last IR line assignments but also Raman assignments in order to consider all available experimental data. A second set of weaker and less isolated line assignments was possible, based on the refined simulation, followed by a new fit, and so on.

In the end, we were able to assign many more lines (almost twice as many; see Table 1) than in our multiisotopic study[27] and over a wider spectral range. We could assign lines up to much higher rotational quantum number values, i.e., $J = 91$, than in ref 27, for which assignments stopped at $J = 79$. The sampling of the rovibrational levels is thus better, which means that the ν_1 and ν_3 Hamiltonian parameters are more reliable. The result is convincing, as shown in Figures 2 and 3 by a comparison of the experimental and simulated spectra.

Table 1. Fit Statistics for the Determination of the $^{192}OsO_4$ Effective Hamiltonian Parameters

	no. of data	J_{max}	$d_{RMS}/10^{-3}$ cm^{-1}
ν_1/ν_3	177 Raman + 1231 IR	91	1.304
ν_2/ν_4	328	88	2.725

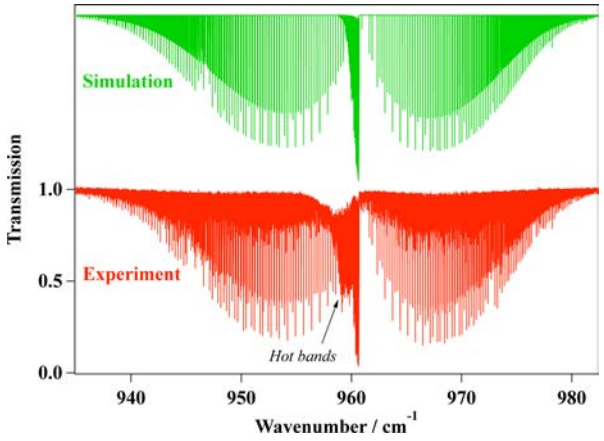

Figure 2. Overview of the ν_1/ν_3 IR region compared to the simulation. The presence of hot bands is indicated to specify the differences between both spectra.

For the simulated spectrum, we used the ν_3 dipole moment derivative from McDowell et al.[38] in order to compute absorption intensities.

The resulting effective Hamiltonian parameters are given in Table 4 of the Appendix.

Bending Dyad Analysis. The bending dyad spectrum study was particularly tricky compared to the previous one. Indeed, the ν_2/ν_4 region is extremely dense even if the spectrum was obtained from a monoisotopic sample: many lines overlap and mix with other branches, and hot bands are also numerous. The tetrahedral splitting is also much bigger than that for the

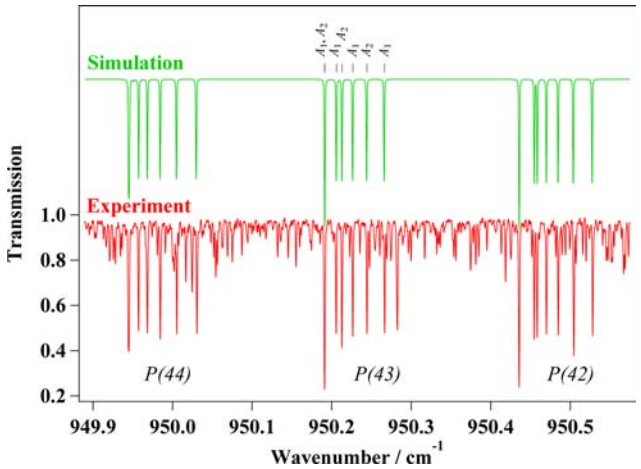

Figure 3. Detail in the *P* branch of the ν_1/ν_3 IR region compared to the simulation. The rotational assignments and upper state symmetries in the $P(43)$ cluster of lines are indicated below the observed spectrum and above the simulation, respectively. They illustrate the so-called tetrahedral splitting, which is moderate for this band because the different J clusters do not overlap. The additional strong line in the $P(43)$ cluster and other weaker lines between the clusters that do not appear in the simulation are hot band lines.

stretching region. A preliminary simulation was performed from four ν_2 and ν_4 Hamiltonian parameters. ν_2 and ν_4 band centers were found in Huston's[40] and McDowell's[38] works, respectively, while two Coriolis parameters (related to the ν_4 and ν_2/ν_4 coupling) were determined from formulas in the literature (see McDowell's,[25] Scappini's,[41] and Loëte's[42] works), as explained in section 6 of our first paper.[27] For the simulated spectrum, the line intensities were only relative (we did not try to compute the absolute intensities at this stage); i.e., the ν_4 dipole moment derivative was arbitrarily fixed to 1. The first set of line assignments was very difficult, so we were obliged to modify some parameters "manually" ($t^{2(2,0E)F_2,F_2}_{\{\nu_4\}\{\nu_4\}}$ and $t^{2(2,0F_2)F_2,F_2}_{\{\nu_4\}\{\nu_4\}}$) to get the first assigned lines. From that point on, we tried to join step by step the assigned line regions, and what is surprising here is that the ν_2 lines are, in fact, intense and easy to assign, although they are not IR-active in the first approximation. They gain intensity through the ν_2/ν_4 Coriolis coupling.

Finally, we did not achieve a full assignment of the spectrum; there still exist some "holes" not assigned, as shown in Figures 5 and 6. Figure 4 shows an overview of the comparison between the experimental and calculated spectra, while a detail is shown in Figure 5. Figure 6 shows the position difference in the wavenumber unit between the experimental and calculated lines for each assignment. Some regions remain too blurred for unambiguous assignment, such as the region displayed in Figure 5. There, weak lines could not be assigned because of the presence of hot bands in the experimental spectrum. As a matter of fact, at room temperature, only 30% of the population lies in the ground state (see Figure 11 and the explanation in the Appendix), which means that 70% are in excited states, hence, the strong contribution of the hot bands. However, the result is globally satisfying because the number of measured levels is reasonable and these are fairly spread over the rovibrational energy levels (see Table 1 and Figure 7). Again, the effective Hamiltonian parameters are given in Table 4 of the Appendix.

dx.doi.org/10.1021/ic3015282 | *Inorg. Chem.* 2012, 51, 10356–10365

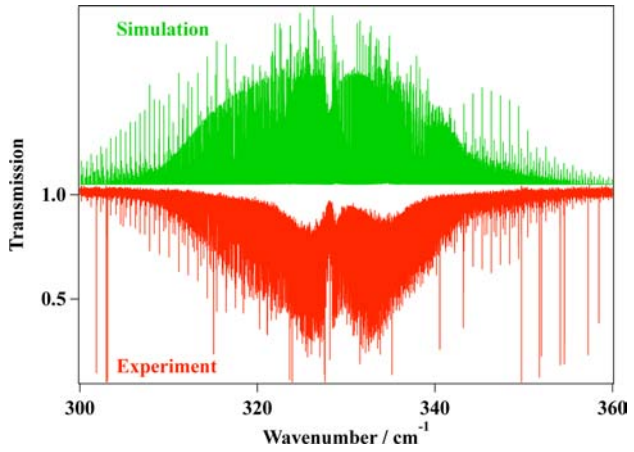

Figure 4. Overview of the ν_2/ν_4 IR region compared to the simulation. Additional H_2O lines appear because of its presence in the cell (checked on the HITRAN[39] database).

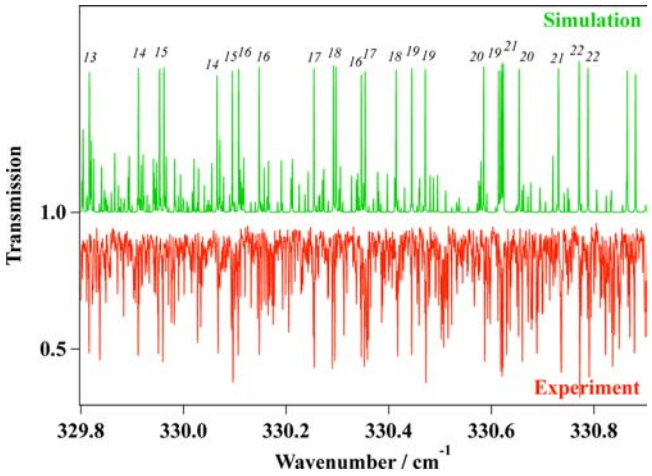

Figure 5. Detail in the *R* branch of the ν_2/ν_4 region, compared to the simulation, with some lower state *J* values indicated.

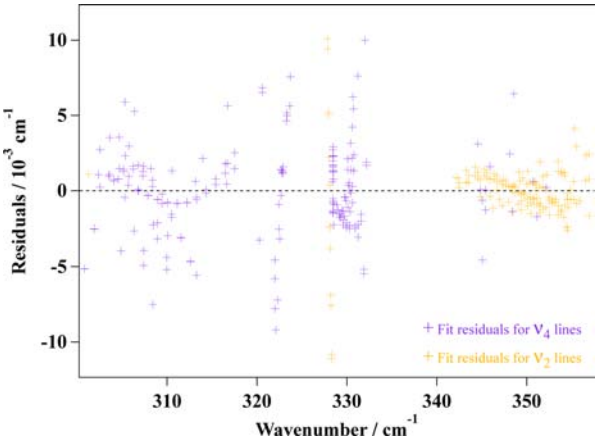

Figure 6. Fit residuals for the IR bending dyad spectrum.

RESULTS AND DISCUSSION

We can now discuss four outcomes of this work. The first one concerns the missing interactions between the stretching and bending levels. Then we discuss the isotopic shifts and the integrated band intensities. Finally, we calculate the Os−O equilibrium bond length.

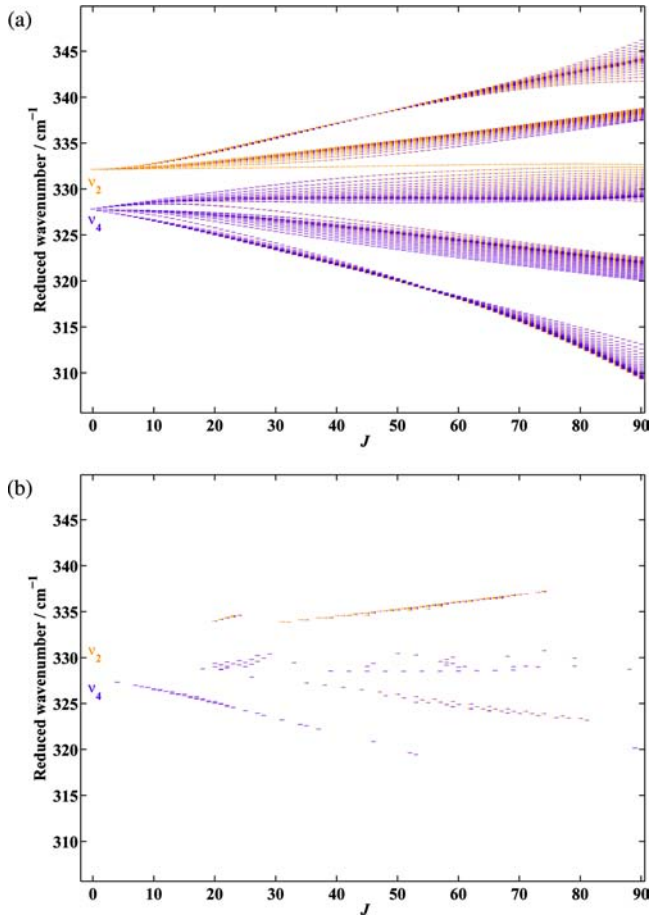

Figure 7. (a) Calculated rovibrational reduced energy levels of the bending dyad, as a function of the rotational quantum number *J*. (b) Rovibrational energy levels of the bending dyad associated with assigned transitions.

Interaction between the Stretching Dyad and the 3-Quanta Bending Polyad. Strictly speaking and considering the approximate relationship $\nu_1 \simeq \nu_3 \simeq 3\nu_2 \simeq 3\nu_4$, the two stretching fundamentals are part of the complex hexad, namely, $\nu_1/\nu_3/3\nu_2/2\nu_2 + \nu_4/\nu_2 + 2\nu_4/3\nu_4$. However, as described in the Theoretical Model section, this hexad analysis has been reduced to the ν_1/ν_3 stretching dyad only because the $3\nu_2/2\nu_2 + \nu_4/\nu_2 + 2\nu_4/3\nu_4$ bending polyad (or the 3-quanta bending polyad) relies on the ν_2 and ν_4 parameters. Before the present work, we did not have enough ν_2/ν_4 parameters and they were only determined approximately, as described above. Thus, we could not include them in the theoretical model to simulate the 3-quanta bending polyad spectrum. Moreover, the tensorial formalism used here is based on a recursive method for polyad construction (the so-called "vibrational extrapolation method"[29,35]); i.e., it requires the analysis and determination of lower vibrational states relative to the considered modes (here, the ν_2 and ν_4 modes). Thus, before analysis of the entire hexad, we need to study correctly the ν_2/ν_4 dyad and also the $2\nu_2/\nu_2 + \nu_4/2\nu_4$ triad (the 2-quanta bending polyad).

The weird behavior observed in Figure 8 showing fit residuals for the stretching dyad spectrum can be explained by this lack of interaction terms between this dyad and the 3-quanta bending polyad in the theoretical model. Indeed, Figure 9 shows that the energy levels of the 3-quanta bending polyad cross those of the stretching dyad exactly in the same zones where the "streaks"

dx.doi.org/10.1021/ic3015282 | Inorg. Chem. 2012, 51, 10356−10365

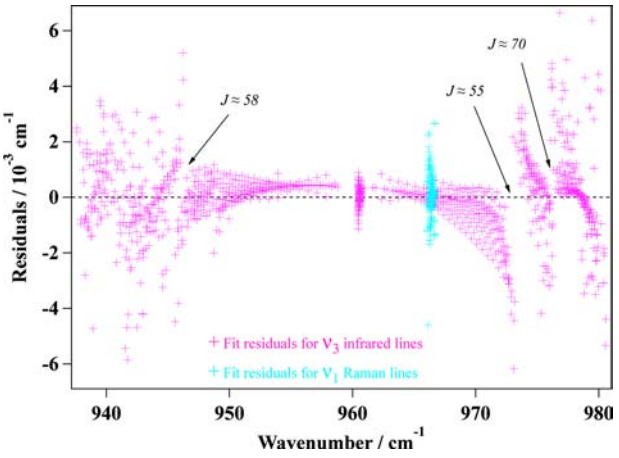

Figure 8. Fit residuals for the IR stretching dyad spectrum. Some regions showing the effect due to missing interaction terms are shown and should be compared to the level crossings shown in Figure 9.

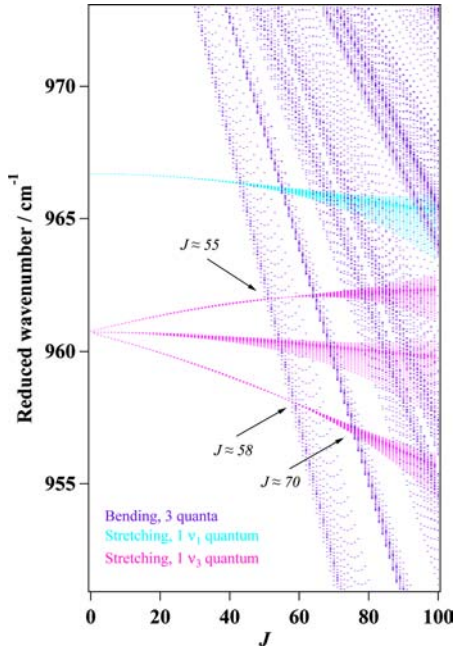

Figure 9. Interaction between the energy levels of the stretching dyad and the 3-quanta bending polyad.

appear in Figure 8. This highlights the fact that, as predicted, interactions are missing in our study and should be taken into account.

However, the study of the bending triad spectrum is not yet feasible for the moment because its lines are too weak to be assigned, as observed at the Synchrotron SOLEIL during the bending dyad recording. The situation would be even worse for the 3-quanta bending tetrad region, again much weaker. Besides, the ν_2 and ν_4 parameter set obtained in the bending dyad study is not sufficiently complete and reliable because the simulation does not match the experimental spectrum exactly and homogeneously. The low-order parameters (band center and rotational constants) are certainly reliable enough for the present structural analysis (see the next sections), but higher order parameters are determined not well enough to allow a correct vibrational extrapolation to the next polyads, precluding at present their detailed spectroscopic investigation.

At first, to improve this study, a "cold" spectrum of the bending dyad should be recorded so that the hot band intensity decreases, making the assignment easier and more accurate. Thus, the ν_2 and ν_4 refined parameters should become more precise. Our first estimation predicts that around 210 K, the temperature that could be reached in a static cold cell that is under development at the Synchrotron SOLEIL, 60% of the population lies in the ground state, whereas the $\nu_2 = 1$ and $\nu_4 = 1$ populations are the same as those at room temperature (see Figure 11 in the Appendix). This means that the ν_2 and ν_4 lines should be twice as intense compared to the hot bands in the bending dyad spectrum. Of course, a supersonic jet expansion would be even better to simplify the spectrum, but this is hard to implement with such a toxic species.

Isotopic Shifts. From this work, together with the results of our multiisotopic studies,[27,28] we can deduce isotopic shifts of the four band centers (see Table 2). This corresponds to the slope of

Table 2. Isotopic Shifts for the Four Band Centers (amu: Atomic Mass Unit)

values/cm^{-1} (amu)			
$\Delta\nu_1$	$\Delta\nu_2$	$\Delta\nu_3$	$\Delta\nu_4$
0.3193 (24)	−0.0291 (18)	−0.267338 (51)	−0.0540 (38)

the band center parameter as a function of the atomic mass number, as obtained through a linear regression fit. These shifts can be used to estimate the spectrum of the other isotopologues.

The $\Delta\nu_1$ and $\Delta\nu_3$ isotopic shifts correspond to the average shift between the isotopologue band center values determined through the stimulated Raman spectrum study[28] and the stretching dyad multiisotopic spectrum study,[27] respectively.

Regarding the $\Delta\nu_2$ and $\Delta\nu_4$ isotopic shifts, their determination was a bit different because we could not assign lines of the multiisotopic bending dyad spectrum (see section 6 of our previous study[27]). However, this spectrum helped us in another way. As expounded in the Bending Dyad Analysis section, many of the ν_2 lines were assigned, particularly in the *R* branch (see Figure 6), which allows us to determine the $\Delta\nu_2$ isotopic shift "manually". From a pattern composed of four lines corresponding to the ones of the four major isotopologues ($^{192}OsO_4$, $^{190}OsO_4$, $^{189}OsO_4$ and $^{188}OsO_4$) and which was repeated in the *R* branch, we performed an average on the shift between the pattern lines for several patterns (see Figure 10). The same procedure was used in the *P* branch for determination of the $\Delta\nu_4$ isotopic shift.

It should be noticed here that the $\Delta\nu_1$ isotopic shift has an anomalous value. Indeed, the reduced mass and thus the harmonic wavenumber for this totally symmetric stretching mode does not depend, in a first approximation, on the mass of the central atom. This implies that the band center value should not change from an isotopologue to another. However, the observed $\Delta\nu_1$ isotopic shift is not zero. As explained in our Raman study,[28] this behavior indicates that the ν_1 parameter is strongly affected by the coupling with the 3-quanta bending polyad described in the previous section.

Integrated Band Intensities. From the low-resolution data presented in the Experimental Details section, one obtains an integrated intensity value of 6.3 ± 0.6 km mol^{-1} for the ν_2/ν_4 bending region. Our measured value is about a factor of 4 smaller than the best ab initio prediction (24.6 km mol^{-1} 15). This corresponds to a summation over all isotopic species, for fundamental and hot-band contributions that may introduce a

dx.doi.org/10.1021/ic3015282 | *Inorg. Chem.* 2012, 51, 10356−10365

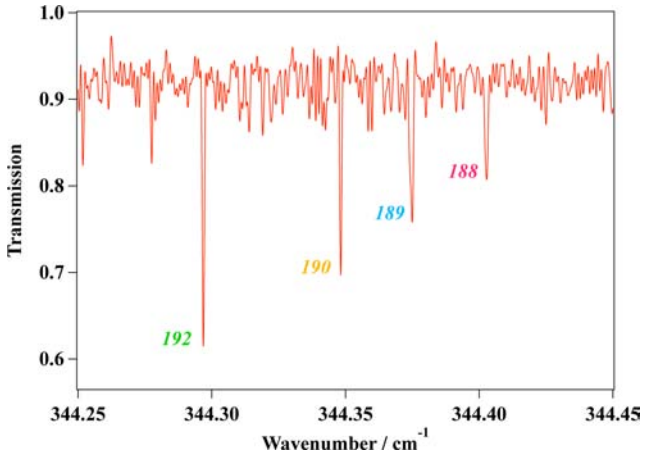

Figure 10. Detail in the *R* branch of the multiisotopic bending dyad spectrum showing lines used for determination of the $\Delta\nu_2$ isotopic shift (the isotopologue atomic mass number is indicated).

very slight deviation in the true fundamental integrated intensity. A similar measurement was thus carried out later in the mid-IR region. It provides a check in the case where an intensity measurement had been made on isolated lines and thus quantitative comparisons could be made of these deviations.

Our measurements for the ν_1/ν_3 stretching region give a value of 104 ± 10 km mol^{-1} for the whole region, in good agreement with the 107 km mol^{-1} value extrapolated for the ν_3 fundamental by McDowell et al.[38] from single-line measurements. As pointed out in ref 19, the predicted IR intensities are quite different from the first approximate measurements.[25] These new data should be useful in serving as reference points for predictions of molecular polarizability.[19,21]

Os−O Bond-Length Calculation at Equilibrium. The essential aim of the analysis of the four fundamental modes was determination of the effective Hamiltonian parameters needed for the Os−O bond-length calculation at equilibrium (r_e). For a tetrahedral molecule like OsO_4, the O−Os−O bond angles are fixed to 109.47° [2 arccos$(1/\sqrt{3})$] and r_e is the only parameter that fully defines the molecular structure. This calculation, based on the expression of the moment of inertia of the molecule, is given by the following expression:

$$r_e = \sqrt{\frac{3h}{64\pi^2 c m_O B_e}} \tag{9}$$

with Planck's constant $h = 6.62606896(33) \times 10^{-34}$ m^2 kg s^{-1},[43] the speed of light in a vacuum $c = 299792458$ m s^{-1},[43] the oxygen mass $m_O = 15.9994$,[43] and the rotational constant at equilibrium B_e. The values are taken from the *IUPAC Green Book*.[43]

B_e depends on some fitted Hamiltonian parameter for each band through the relationship

$$B_e = B_0 + \sum_{i=1}^{4} \alpha_i \frac{d_i}{2} \tag{10}$$

where

$$\alpha_i = -\Delta B_i = -t^{2(0,A_1)\Gamma_i\Gamma_i}_{\{i\}\{i\}} = B_0 - B_i \tag{11}$$

with i the index of normal modes ($i = 1-4$), d_i the degeneracy of the i mode (see the Theoretical Model section), and B_0 (ground-state rotational constant) and $t^{2(0,A_1)\Gamma_i\Gamma_i}$ the fitted parameters referred to in Table 4 of the Appendix. The B_i values are the upper-state rotational constants. Finally, we get

$$r_e = 1.70919(16)\ \text{Å} \tag{12}$$

This result increases markedly the precision of the experimental bond-length determination with respect to the results of previous studies by Seip and Stølevik[23] and Díaz-Moreno and Bowron.[24] As seen in Table 3, the spread in ab initio predictions is rather large (0.1 Å) compared to the present determination, which can be used as a precise reference point.

Table 3. Comparison of the Os−O Bond-Length Values at Equilibrium with Previous Works

ref	r_e/Å	technique
this work	1.70919(16)	HR spectroscopy (gas phase)
22	1.74(2)	X-ray diffraction (solid phase)
23	1.711(3)	electron diffraction (gas phase)
24	1.712(3)	EXAFS (gas phase)
15	1.785	ab initio calculation [MP2/6-31G(d)]
16	1.66	ab initio calculation (Hartree−Fock)
16	1.70	ab initio calculation (relativistic Dirac−Fock)
20	1.738	ab initio calculation (relativistic MP2)
20	1.738	relativistic DFT calculation
21	1.76	DFT calculation

CONCLUSION

The HR spectroscopic analysis of the four fundamentals, with IR spectra for the ν_3 and ν_2/ν_4 bands and a Raman spectrum for the ν_1 band, allowed us to estimate a very precise value of the Os−O bond length at equilibrium. This result could serve as a benchmark for ab initio calculations because those methods are still not efficient enough for molecules containing such a heavy metal.

At present, the only possibility of improving further the precision of the structural determination would be to increase the number of assigned lines in the analysis. This could be done, for instance, by working at lower temperature to increase the ground-state population and decrease the hot-band interferences but would require considerable experimental developments and bring a relatively small improvement with regard to the present bond-length uncertainty and the large existing spread in ab initio predictions.

Finally, we plan to fit the effective dipole moment using the experimental intensities of the assigned lines. To do that, we require well-isolated lines to measure their intensities. The stretching dyad spectrum is thus a good candidate. Moreover, it is intense and situated in an interesting region of the IR spectrum (mid-IR) for a possible in situ detection of OsO_4. To obtain reliable effective dipole moment parameter values, spectra with different pressures should be recorded. Such a study could serve for the precise determination of the OsO_4 concentration in the atmosphere, near car exhaust pipes, in industrial environments, etc.

APPENDIX

Effective Hamiltonian Parameters of $^{192}OsO_4$

The effective Hamiltonian parameters resulting from the present ν_1/ν_3 and ν_2/ν_4 spectral fits are given in Table 4.

dx.doi.org/10.1021/ic3015282 | Inorg. Chem. 2012, 51, 10356−10365

Table 4. Effective Hamiltonian Parameters of the $^{192}OsO_4$ Molecule

		parameter				
polyad	order	$\Omega(K,nC)$	$\{s\}$ C_1	$\{s'\}$ C_2	value/cm^{-1}	"usual" notation; see ref 35
GS	0	$2(0,0A_1)$	$0000A_1$	$0000A_1$	$1.3489628558 \times 10^{-1}$[a]	B_0
GS	2	$4(0,0A_1)$	$0000A_1$	$0000A_1$	$-2.7272238705 \times 10^{-8}$[a]	$-D_0$
GS	2	$4(4,0A_1)$	$0000A_1$	$0000A_1$	$-1.4063502350 \times 10^{-9}$[a]	$-[(15)^{1/2}/4\sqrt{2}]D_{0t}$
GS	4	$6(0,0A_1)$	$0000A_1$	$0000A_1$	$-8.6285563672 \times 10^{-14}$[a]	H_0
GS	4	$6(4,0A_1)$	$0000A_1$	$0000A_1$	$4.3964762573 \times 10^{-14}$[a]	$(3\sqrt{5}/16\sqrt{2})H_{4t}$
GS	4	$6(6,0A_1)$	$0000A_1$	$0000A_1$	$8.0219960881 \times 10^{-16}$[a]	$-[(231)^{1/2}/64\sqrt{2}]H_{4t}$
GS	6	$8(0,0A_1)$	$0000A_1$	$0000A_1$	$7.3263880190 \times 10^{-18}$[a]	L_0
GS	6	$8(4,0A_1)$	$0000A_1$	$0000A_1$	0.0[a]	$-[3(15)^{1/2}/64\sqrt{2}]L_{4t}$
GS	6	$8(6,0A_1)$	$0000A_1$	$0000A_1$	0.0[a]	$[3(77)^{1/2}/256\sqrt{2}]L_{6t}$
GS	6	$8(8,0A_1)$	$0000A_1$	$0000A_1$	0.0[a]	$[1/32(33)^{1/2}]L_{8t}$
ν_1/ν_3	0	$0(0,0A_1)$	$1000A_1$	$1000A_1$	966.69398(17)	ν_1
ν_1/ν_3	2	$2(0,0A_1)$	$1000A_1$	$1000A_1$	$-1.8989(17) \times 10^{-4}$	$B_1 - B_0$
ν_1/ν_3	2	$2(2,0F_2)$	$1000A_1$	$0010F_2$	$9.67(13) \times 10^{-5}$	$(3/4\sqrt{2})d_{13}$ ($\nu_1 - \nu_3$ Coriolis)
ν_1/ν_3	0	$0(0,0A_1)$	$0010F_2$	$0010F_2$	960.739151(82)	ν_3
ν_1/ν_3	1	$1(1,0F_1)$	$0010F_2$	$0010F_2$	$7.14800(32) \times 10^{-2}$	$3\sqrt{2}B\zeta_3$ (ν_3 Coriolis)
ν_1/ν_3	2	$2(0,0A_1)$	$0010F_2$	$0010F_2$	$-1.7001(12) \times 10^{-4}$	$B_3 - B_0$
ν_1/ν_3	2	$2(2,0E)$	$0010F_2$	$0010F_2$	$2.211(17) \times 10^{-5}$	$-(1/2)\alpha^3_{220} - 6\alpha^3_{224}$
ν_1/ν_3	2	$2(2,0F_2)$	$0010F_2$	$0010F_2$	$-9.183(25) \times 10^{-5}$	$-(3/4)\alpha^3_{220} + 6\alpha^3_{224}$
ν_1/ν_3	3	$3(1,0F_1)$	$0010F_2$	$0010F_2$	$1.303(35) \times 10^{-8}$	$-(3\sqrt{3/4}\sqrt{2})F^3_{110}$
ν_1/ν_3	3	$3(3,0F_1)$	$0010F_2$	$0010F_2$	$-2.915(26) \times 10^{-8}$	$(3/\sqrt{5/2})F^3_{134}$
ν_1/ν_3	4	$4(0,0A_1)$	$0010F_2$	$0010F_2$	$-1.47(62) \times 10^{-10}$	$-(D_3 - D_0)$
ν_1/ν_3	4	$4(2,0E)$	$0010F_2$	$0010F_2$	$1.18(67) \times 10^{-10}$	$\sqrt{3/8}G^3_{220} + 3\sqrt{3/2}G^3_{224}$
ν_1/ν_3	4	$4(2,0F_2)$	$0010F_2$	$0010F_2$	$-2.82(59) \times 10^{-10}$	$3\sqrt{3/16}G^3_{220} - 3\sqrt{3/2}G^3_{224}$
ν_1/ν_3	4	$4(4,0A_1)$	$0010F_2$	$0010F_2$	$6.9(1.2) \times 10^{-11}$	$-3\sqrt{5/4}\sqrt{2}(D_{3t} - D_{0t})$
ν_1/ν_3	4	$4(4,0E)$	$0010F_2$	$0010F_2$	$1.07(30) \times 10^{-10}$	$-3\sqrt{7/2}G^3_{244} + (21)^{1/2}/2(22)^{1/2}G^3_{246}$
ν_2/ν_4	0	$0(0,0A_1)$	$0100F_2$	$0100F_2$	332.14481(81)	ν_2
ν_2/ν_4	2	$2(0,0A_1)$	$0100E$	$0100E$	$1.68(11) \times 10^{-4}$	$B_2 - B_0$
ν_2/ν_4	2	$2(2,0E)$	$0100E$	$0100E$	$3.86(94) \times 10^{-5}$	$\sqrt{3}b_2 + 24(\sqrt{3/7})C_6$
ν_2/ν_4	3	$3(3,0A_2)$	$0100E$	$0100E$	$1.97(38) \times 10^{-7}$	$1/2d_2$
ν_2/ν_4	4	$4(0,0A_1)$	$0100E$	$0100E$	$-1.631(79) \times 10^{-8}$	$-(D_2 - D_0)$
ν_2/ν_4	4	$4(2,0E)$	$0100E$	$0100E$	$7.54(33) \times 10^{-9}$	$-3/4C_5 + 9/7C_6$
ν_2/ν_4	1	$1(1,0F_1)$	$0100E$	$0001F_2$	$-2.6002(43) \times 10^{-1}$	$-\sqrt{3}R_{24} + \sqrt{3/10}F_{24}$
ν_2/ν_4	2	$2(2,0F_2)$	$0100E$	$0001F_2$	$-2.316(76) \times 10^{-4}$	$3\sqrt{8}d_{24}$
ν_2/ν_4	3	$3(1,0F_1)$	$0100E$	$0001F_2$	$-7.39(51) \times 10^{-7}$	$3/4R^{01}_{24} + 3/4F_{24} + 9/80F_{24}$
ν_2/ν_4	3	$3(3,0F_1)$	$0100E$	$0001F_2$	$-2.28(36) \times 10^{-7}$	$-\sqrt{3/4}(10)^{1/2}F_{24}$
ν_2/ν_4	3	$3(3,0F_2)$	$0100E$	$0001F_2$	$-5.67(23) \times 10^{-7}$	$\sqrt{3/2}\sqrt{2}F_{24}$
ν_2/ν_4	4	$4(2,0F_2)$	$0100E$	$0001F_2$	$1.186(36) \times 10^{-8}$	
ν_2/ν_4	4	$4(4,0F_1)$	$0100E$	$0001F_2$	$1.000(18) \times 10^{-8}$	
ν_2/ν_4	4	$4(4,0F_2)$	$0100E$	$0001F_2$	$2.474(34) \times 10^{-8}$	
ν_2/ν_4	0	$0(0,0A_1)$	$0001F_2$	$0001F_2$	327.84144(40)	ν_4
ν_2/ν_4	1	$1(1,0F_1)$	$0001F_2$	$0001F_2$	$2.07818(39) \times 10^{-1}$	$3\sqrt{2}B\zeta_4$ (ν_4 Coriolis)
ν_2/ν_4	2	$2(0,0A_1)$	$0001F_2$	$0001F_2$	$-1.161(79) \times 10^{-4}$	$B_4 - B_0$
ν_2/ν_4	2	$2(2,0E)$	$0001F_2$	$0001F_2$	$2.54(11) \times 10^{-4}$	$-(1/2)\alpha^4_{220} - 6\alpha^4_{224}$
ν_2/ν_4	2	$2(2,0F_2)$	$0001F_2$	$0001F_2$	$-1.643(86) \times 10^{-4}$	$-(3/4)\alpha^4_{220} + 6\alpha^4_{224}$
ν_2/ν_4	3	$3(1,0F_1)$	$0001F_2$	$0001F_2$	$1.133(48) \times 10^{-6}$	$-(3\sqrt{3/4}\sqrt{2})F^4_{110}$
ν_2/ν_4	3	$3(3,0F_1)$	$0001F_2$	$0001F_2$	$6.39(49) \times 10^{-7}$	$(3/\sqrt{5/2})F^4_{134}$
ν_2/ν_4	4	$4(0,0A_1)$	$0001F_2$	$0001F_2$	$-8.77(79) \times 10^{-9}$	$-(D_4 - D_0)$
ν_2/ν_4	4	$4(2,0E)$	$0001F_2$	$0001F_2$	$-2.901(75) \times 10^{-8}$	$\sqrt{3/8}G^4_{220} + 3\sqrt{3/2}G^4_{224}$
ν_2/ν_4	4	$4(2,0F_2)$	$0001F_2$	$0001F_2$	$2.601(40) \times 10^{-8}$	$3\sqrt{3/16}G^4_{220} - 3\sqrt{3/2}G^4_{224}$
ν_2/ν_4	4	$4(4,0A_1)$	$0001F_2$	$0001F_2$	$1.20(16) \times 10^{-9}$	$-3\sqrt{5/4}\sqrt{2}(D_{4t} - D_{0t})$
ν_2/ν_4	4	$4(4,0E)$	$0001F_2$	$0001F_2$	$2.336(39) \times 10^{-8}$	$-3\sqrt{7/2}G^4_{244} + (21)^{1/2}/2(22)^{1/2}G^4_{246}$
ν_2/ν_4	4	$4(4,0F_2)$	$0001F_2$	$0001F_2$	$2.190(20) \times 10^{-8}$	$-9\sqrt{7/8}G^4_{244} - (21)^{1/2}/(22)^{1/2}G^4_{246}$

[a]Fixed value.

Vibrational Energy-Level Populations

In order to estimate the importance of hot bands at a given temperature T, we can calculate the population of the different vibrational energy levels. For a given vibrational state with quantum numbers $\{v_i, i = 1, 4\}$, its energy in the harmonic approximation (which is sufficient for the present purpose) is

dx.doi.org/10.1021/ic3015282 | Inorg. Chem. 2012, 51, 10356−10365

$$E = hc\sum_{i=1}^{4}\tilde{\nu}_i\nu_i \tag{13}$$

with $\tilde{\nu}_i$ being the harmonic oscillator wavenumbers of each normal mode (966.69, 332.14, 960.740, and 327.84 cm^{-1} for i = 1−4, respectively, as taken from Table 4). The zero-point energy has been set to zero. In this approximation, the vibrational partition function is expressed as

$$Q = \prod_{i=1}^{4}(1 - e^{-hc\tilde{\nu}_i/kT})^{-d_i} \tag{14}$$

where d_i = 1, 2, 3, 3 for i = 1−4, respectively, is the degeneracy of each normal-mode oscillator, k is Boltzmann's constant, h is Planck's constant, and c is the speed of light. The total degeneracy of the vibrational level is given by

$$D = (\nu_2 + 1)(\nu_3 + 1)(\nu_3 + 2)(\nu_4 + 1)(\nu_4 + 2)/4 \tag{15}$$

Then, the population of the considered vibrational level is

$$P = \frac{De^{-E/kT}}{Q} \tag{16}$$

Figure 11 displays P as a function of T for the lowest vibrational levels of $^{192}OsO_4$. In particular, it shows that the room temperature population of the ground state is only 30% and also that hot bands are dominated by transitions starting from the ν_2 = 1 and ν_4 = 1 vibrational levels.

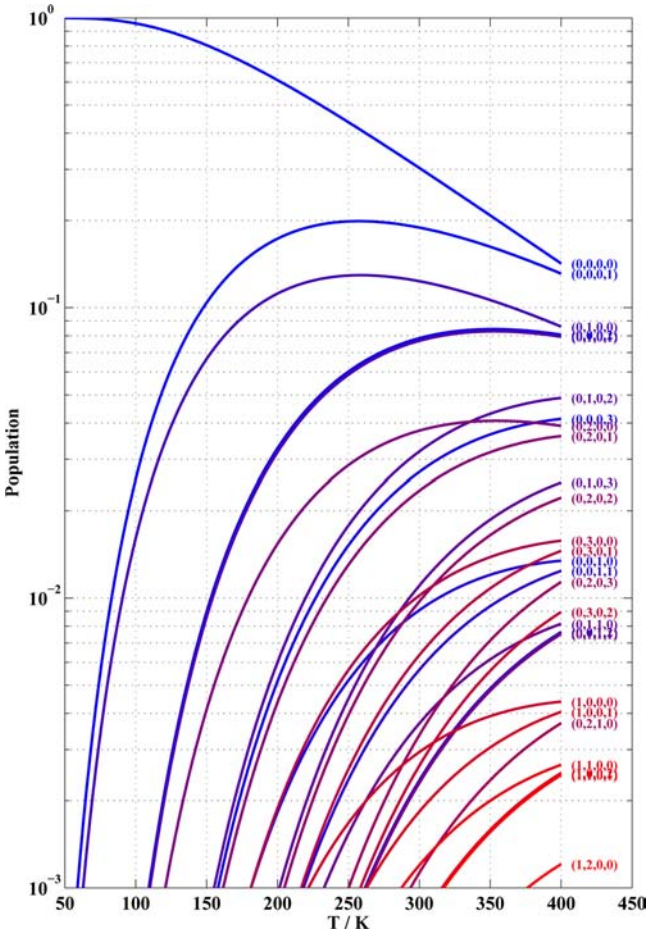

Figure 11. Population of the $^{192}OsO_4$ vibrational states as a function of the temperature. Vibrational-level labels are indicated on the right in the form of (ν_1, ν_2, ν_3, ν_4).

AUTHOR INFORMATION

Corresponding Author

*E-mail: Maud_Louviot@etu.u-bourgogne.fr.

Notes

The authors declare no competing financial interest.

ACKNOWLEDGMENTS

The authors thank Prof. Hans-Rudolf Jauslin (ICB, Dijon, France) for his help in correcting the manuscript and his useful suggestions.

REFERENCES

(1) Rauch, S.; Hemond, H. F.; Feucker-Ehrenbrink, B. *Environ. Sci. Technol.* **2004**, *38*, 396−402.
(2) Rodushkin, I.; Engström, E.; Sörlin, D.; Baxter, D.; Hörnfeldt, B.; Nyholm, E.; Eckek, F. *Water Air Soil Pollut.* **2011**, *218*, 603−610.
(3) Barbante, C.; Veysseyre, A.; Ferrari, C.; Van de Velde, K.; Morel, C.; Capodaglio, G.; Cescon, P.; Scarponi, G.; Boutron, C. *Environ. Sci. Technol.* **2001**, *35*, 835−839.
(4) Švorc, L.; Tomčik, P.; Durdiak, J.; Rievaj, M.; Bustin, D. *Polym. J. Environ. Stud.* **2012**, *21*, 7−13.
(5) Poirier, A.; Gariépy, C. *Environ. Sci. Technol.* **2005**, *39*, 4431−4434.
(6) Makarovsky, I.; Markel, G.; Hoffman, A.; Schein, O.; Finkelstein, A.; Brosh-Nissimov, T.; Tashma, Z.; Dushnitsky, T.; Eisenkraft, A. *Isr. Med. Assoc. J.* **2007**, *9*, 750−752.
(7) Criegee, R.; Marchand, B.; Wannowius, H. *Justus Liebigs Ann. Chem.* **1942**, *550*, 99−133.
(8) Parameswaran, S.; Verma, R. S. *Anal. Biochem.* **2011**, *416*, 186−190.
(9) Théron, L.; Astruc, T.; Bouillier-Oudot, M.; Molette, C.; Vénien, A.; Peyrin, F. *Meat Sci.* **2011**, *89*, 377−383.
(10) Schröder, M. *Chem. Rev.* **1980**, *80*, 187−213.
(11) Cui, J.; Burghard, M.; Kern, K. *Nano Lett.* **2003**, *3*, 613−615.
(12) Hasell, T.; Schmidtmann, M.; Cooper, A. I. *J. Am. Chem. Soc.* **2011**, *133*, 14920−14923.
(13) Hawkins, J. M.; Meyer, A.; Lewis, T. A.; Loren, S.; Hollander, F. J. *Science* **1991**, *252*, 312−313.
(14) Autschbach, J. *J. Chem. Phys.* **2012**, *136*, 150902.
(15) Veldkamp, A.; Frenking, G. *Chem. Ber.* **1993**, *126*, 1325−1330.
(16) Malli, G. L. *J. Chem. Phys.* **2002**, *117*, 10441−10443.
(17) Düllmann, B. E.; Eichler, R.; Gäggler, H. W.; Türler, A. *J. Phys. Chem. B* **2002**, *106*, 6679−6684.
(18) Filatov, M.; Cremer, D. *J. Chem. Phys.* **2003**, *119*, 1412−1420.
(19) Hohm, U.; Maroulis, G. *J. Chem. Phys.* **2004**, *121*, 10411−10418.
(20) Filatov, M.; Cremer, D. *J. Chem. Phys.* **2005**, *122*, 044104.
(21) Pershina, V.; Bastug, T.; Fricke, B. *J. Chem. Phys.* **2005**, *122*, 124301.
(22) Ueki, T.; Zaikin, A.; Templeton, D. H. *Acta Crystallogr.* **1965**, *19*, 157−160.
(23) Seip, H. M.; Stølevik, R. *Acta Chem. Scand.* **1966**, *20*, 385−394.
(24) Díaz-Moreno, S.; Bowron, D. T. *Organometallics* **2003**, *22*, 390−394.
(25) McDowell, R. S.; Goldblatt, M. *Inorg. Chem.* **1971**, *10*, 625−630.
(26) Bobin, B.; Valentin, A.; Henry, L. *J. Mol. Spectrosc.* **1987**, *122*, 229−241.
(27) Louviot, M.; Boudon, V.; Manceron, L.; Roy, P.; Balcon, D. *J. Quant. Spectrosc. Radiat. Transfer* **2012**, *113*, 119−127.
(28) Louviot, M.; Boudon, V.; Bermejo, D.; Martínez, R. Z.; Manceron, L. *J. Raman Spectrosc.* **2012**.
(29) Boudon, V.; Champion, J.-P.; Gabard, T.; Loëte, M.; Rotger, M.; Wenger, C. In *Handbook of High-Resolution Spectroscopy*; Quack, M., Merkt, F., Eds.; Wiley: New York, 2011; Vol. 3; pp 1437−1460.
(30) Roy, P.; Rouzières, M.; Qi, Z.; Chuba, O. *Infrared Phys. Technol.* **2006**, *49*, 139−146.

(31) Brubach, J.-B.; Manceron, L.; Rouzieres, M.; Pirali, O.; Balcon, D.; Tchana, F. K.; Boudon, V.; Tudorie, M.; Huet, T.; Cuisset, A.; Roy, P. In *WIRMS 2009: 5Th International Workshop on Infrared Microscopy and Spectroscopy with Accelerator Based Sources*; Predoi-Cross, A., Billinghurst, B. E., Eds.; AIP Conference Proceedings; American Institute of Physics: Melville, NY, 2010; Vol. *1214*; pp 81−84.
(32) Boudon, V.; Pirali, O.; Roy, P.; Brubach, J. B.; Manceron, L.; Vander Auwera, J. *J. Quant. Spectrosc. Radiat. Transfer* **2010**, *111*, 1117−1129.
(33) Rothman, L. S.; Jacquemart, D.; Barbe, A.; Benner, D. C.; Birk, M.; Brown, L. R.; Carleer, M. R.; Chackerian, C.; Chance, K.; Coudert, L.; Dana, V.; Malathy-Devi, V.; Flaud, J.-M.; Gamache, R. R.; Goldman, A.; Hartmann, J. M.; Jucks, K. W.; Maki, A. G.; Mandin, J. Y.; Massie, S.; Orphal, J.; Perrin, A.; Rinsland, C. P.; Smith, M. A.; Toth, R. A.; Vander Auwera, J.; Varanasi, P.; Wagner, G. *J. Quant. Spectrosc. Radiat. Trans.* **2005**, *96*, 139−204.
(34) Di Lonardo, G. D.; Fusina, L.; Baldan, A.; Martínez, R. Z.; Bermejo, D. *J. Mol. Phys.* **2011**, *109*, 2533−2542.
(35) Champion, J.-P.; Loëte, M.; Pierre, G. In *Spectroscopy of the Earth's Atmosphere and Interstellar Medium*; Rao, K. N., Weber, A., Eds.; Academic Press: San Diego, 1992; pp 339−422.
(36) Boudon, V.; Champion, J.-P.; Gabard, T.; Loëte, M.; Michelot, F.; Pierre, G.; Rotger, M.; Wenger, C.; Rey, M. *J. Mol. Spectrosc.* **2004**, *228*, 620−634.
(37) Wenger, C.; Boudon, V.; Rotger, M.; Sanzharov, M.; Champion, J.-P. *J. Mol. Spectrosc.* **2008**, *251*, 102−113.
(38) McDowell, R. S.; Radziemski, L. J.; Flicker, H.; Galbraith, H. W.; Kennedy, R. C.; Nereson, N. G.; Krohn, B. J.; Aldridge, J. P.; King, J. D. *J. Chem. Phys.* **1978**, *69*, 1513−1521.
(39) Rothman, L. S.; et al. *J. Quant. Spectrosc. Radiat. Transfer* **2009**, *110*, 533−572.
(40) Huston, J.; Claassen, H. H. *J. Chem. Phys.* **1970**, *52*, 5646−5648.
(41) Scappini, F.; Kreiner, W. A.; Frye, J. M.; Oka, T. *J. Mol. Spectrosc.* **1984**, *106*, 436−440.
(42) Loëte, M. *Can. J. Phys.* **1983**, *61*, 1242−1259.
(43) Cohen, E. R.; Cvitaš, T.; Frey, J. G.; Holmström, B.; Kuchitsu, K.; Marquardt, R.; Mills, I.; Pavese, F.; Quack, M.; Stohner, J.; Strauss, H. L.; Takami, M.; Thor, A. J. *Quantities, units and symbols in physical chemistry*; Royal Society of Chemistry: London, 2007.